

monthly averages also results from the natural variability when few measurements are available.

24. G. F. Herman, J. Curry, *J. Clim. Appl. Meteorol.* **23**, 5 (1984).
25. D. Tanré *et al.*, *Geophys. Res. Lett.*, **28**, 4555 (2001).
26. Each point in Fig. 3 shows the average of individual CDR measurements that correspond to a given bin of aerosol load estimates. Because there is a significant uncertainty on the aerosol load, this average is derived from cases with actual loads that may be higher or lower than the bin value. For the lowest load bin,

only higher loads (smaller CDR) contaminate the estimate. This tends to decrease the average CDR all the more that the uncertainty on the aerosol load is larger.

27. G. Feingold *et al.*, *J. Geophys. Res.* **106**, 22907 (2001).
28. Because the curve as a function of optical thickness (green) is significantly above that as a function of aerosol index (blue), one may get the false impression that they have been obtained from different sets of CDR and aerosol retrievals. In fact, more

than half of aerosol index estimates fall into the lowest load bin when the corresponding optical thicknesses are distributed over a wider range of values. The blue and green curves have been derived from the same sample and have the same overall mean CDR.

29. S. Twomey, in *Atmospheric Aerosols* (Elsevier Science, New York, 1977); see in particular equations 4 to 15.

20 September 2001; accepted 3 January 2002

## Evidence for Strengthening of the Tropical General Circulation in the 1990s

Junye Chen,<sup>1,2\*</sup> Barbara E. Carlson,<sup>2</sup> Anthony D. Del Genio<sup>2</sup>

Satellite observations suggest that the thermal radiation emitted by Earth to space increased by more than 5 watts per square meter, while reflected sunlight decreased by less than 2 watts per square meter, in the tropics over the period 1985–2000, with most of the increase occurring after 1990. By analyzing temporal changes in the frequency of occurrence of emitted thermal and reflected solar fluxes, the effects of El Niño–Southern Oscillation are minimized, and an independent longer-time-scale variation of the radiation budget is identified. Similar analyses of upper tropospheric humidity, cloud amount, surface air temperature, and vertical velocity confirm that these flux changes are associated with a decadal-time-scale strengthening of the tropical Hadley and Walker circulations. Equatorial convective regions have intensified in upward motion and moistened, while both the equatorial and subtropical subsidence regions have become drier and less cloudy.

The energy exchange between Earth and its environment is determined by the emitted thermal [longwave (LW)] flux and the reflected part of the solar irradiance [shortwave (SW)] flux at the top of the atmosphere (TOA). Equilibrium of Earth's climate requires that the global annual mean net radiation flux at the TOA be approximately zero.

Clouds and the Earth's Radiant Energy System (CERES) (1) instruments on the Tropical Rainfall Measuring Mission (TRMM, begun in 1998) satellite and the Earth Observing System Terra (begun in 2000) satellite have observed LW fluxes 5 to 10 W m<sup>-2</sup> (~2 to 4%) higher than those from the Earth Radiation Budget Experiment (ERBE) (2) scanner data (1985–1989). These differences cannot be fully explained by known changes of the satellite observation systems (3–5). The ERBE wide field of view (WFOV) data (1985–1995) span a longer time period though at lower spatial resolution than the ERBE scanner data and clearly show a decadal increase of LW flux, primarily during the first half of the 1990s (3) (Fig. 1).

Local LW changes are weakly positive, about 4 W m<sup>-2</sup> over 10 years, in most of the tropics (6). Much larger changes occur adjacently with opposite sign (for example, the West Pacific warm pool and Central Pacific region).

Empirical orthogonal function (EOF) analysis decomposes temporal variations into orthogonal spatial patterns that sometimes reveal independent physical mechanisms (7). When EOF analysis is applied to the radiation flux anomalies (8), the first principal component (PC) describing the time evolution of the first spatial pattern is strongly correlated with the NINO3 El Niño–Southern Oscillation (ENSO) index (9), and the first spatial pattern explaining the largest fraction of the temporal variance resembles the West Pacific–Central Pacific dipole. This mode is an embodiment

of the well-known shift of the convection center between the two regions in different ENSO phases (10). But the decadal LW flux increase (Fig. 1) cannot be identified by the spatial-temporal EOF decomposition. Although in 1998 both the ENSO index and the tropical mean LW flux anomalies reach their maximum, the two time series are poorly correlated with each other (Fig. 2A). This implies that the mechanism behind the long-term average LW flux increase is distinct from the ENSO phenomenon. The elevated CERES Terra LW flux in 2000, a non-ENSO year, relative to the ERBE period is further evidence for a longer term flux variation.

Because ENSO primarily involves a spatial redistribution, frequency histograms of SW and LW fluxes covering the entire tropics exhibit much less interannual variability than do the geographical distributions of the fluxes within the tropics. We therefore minimize the ENSO signal by constructing a SW-LW joint frequency distribution (JFD) matrix (11) for each month. We then compute anomalies of the JFD with respect to the climatology and decompose these with EOF analysis (12). The high correlation between the first PC and the tropical mean LW flux anomaly time series means that the first mode of the SW-LW JFD EOF represents the long-term increase in LW flux (Fig. 2A). The first PC shows that the increase begins at the start of the 1990s, and elevated flux levels are still present in 2000. The first JFD EOF pattern (Fig. 2B) shows that occurrences of LW flux values of ~255 W m<sup>-2</sup> and SW flux values of ~75 W m<sup>-2</sup> decrease over the 1985–2000 time period and are replaced by higher LW fluxes of ~290 W m<sup>-2</sup> and lower SW fluxes of ~60 W m<sup>-2</sup>. To mimic the effect of a worst-case hypothetical calibration shift in

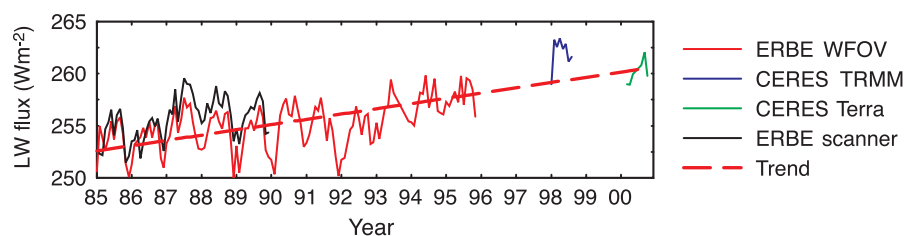


**Fig. 1.** Tropical mean LW flux time series showing decadal variation averaged over 30°S–30°N. The red dashed line is the linear fit to the ERBE WFOV, CERES TRMM, and CERES Terra data. The slope is 3.7 W m<sup>-2</sup> per decade.

<sup>1</sup>Department of Earth and Environmental Sciences, Columbia University, Palisades, NY 10964, USA.

<sup>2</sup>NASA/Goddard Institute for Space Studies, 2880 Broadway, New York, NY 10025, USA.

\*To whom correspondence should be addressed. E-mail: jchen@giss.nasa.gov

## REPORTS

the ERBE WFOV, we multiplied the observed climatology of LW and SW values by 1.01, created the corresponding JFD, and subtracted the actual climatological JFD from the result. This artificial JFD change bears no resemblance to the observed SW anomalies and only resembles the LW anomalies in the Southern Hemisphere subtropics. Thus, we are confident that Earth has been radiating more heat and reflecting less sunlight in the region from 30°S to 30°N over the past decade ( $3.7 \text{ W m}^{-2}$  and  $-0.8 \text{ W m}^{-2}$  per decade, respectively), the net result being more energy leaving the tropics [see also fig. 2 of the companion paper (3) by Wielicki *et al.* in this issue].

The decadal flux variation captured by the first mode should be associated with observable changes in the tropical general circulation. The spatial distribution of radiative fluxes in the tropics is mainly determined by two thermodynamically direct overturning circulations: the Hadley cell in the meridional plane and the Walker cell in the zonal plane along the equator. In convergent regions, deep convection transports water vapor up-

ward, and adiabatically cooled water vapor saturates and generates clouds. Water vapor and clouds absorb the LW flux from the surface and lower troposphere, reducing the TOA LW flux. Clouds reflect SW radiation back to space, increasing the TOA SW flux. In divergent regions, large-scale subsidence warming keeps the free atmosphere dry and relatively cloud-free. Low water vapor concentrations and cloud amounts allow more of the LW flux from the surface and lower troposphere to leak into space, increasing the TOA LW flux. At the same time, the reflected SW flux at the TOA is low because of the small cloud amount.

To further confirm the 1990s TOA radiation flux changes and examine their relationship to potential changes in the tropical atmospheric system, we performed EOF analyses of the JFD of a variety of atmospheric parameters and the TOA LW flux. Based on this, we identified the following key parameters for further investigation: total cloud amount from the International Satellite Cloud Climatology Project D2 data set (13), upper troposphere relative humidity (UTH) from the High-Resolution Infrared Ra-

diation Sounder (HIRS) (14), surface air temperature (SAT) from the GISS analysis of surface temperature (15), pressure vertical velocity [ $\omega$  (16)] at the 500-hPa level from the National Centers for Environmental Prediction/National Center for Atmospheric Research (NCEP) reanalysis (17), and TOA SW flux from the ERBE and CERES data sets. The combined EOF analyses (18) are applied to the JFDs of these five parameters and the TOA LW flux over the common time range for these data sets, from January 1985 to August 1994. The zonal mean Hadley circulation has a relatively fixed rising branch confined to the 10°S–10°N equatorial region and two subsidence branches in the Southern and Northern Hemisphere subtropical regions, 25°S–10°S and 15°N–30°N, respectively. The JFD EOF analysis is applied separately to equatorial and subtropical region data.

In the combined analyses, we select the first EOF for the subtropics and the second EOF for the equatorial region to study. These are the modes whose PC time series exhibit a decadal change and correlate best with the mean tropical LW anomaly time series (Fig. 3, A and B). In the subtropical regions, where the dominant feature is the downwelling branch of the Hadley cell, the shift of LW flux value occurrences from  $\sim 255 \text{ W m}^{-2}$  to  $\sim 285 \text{ W m}^{-2}$  (corresponding to a mean change of  $2.8 \text{ W m}^{-2}$  from January 1985 to August 1994 over the latitude band) (Fig. 4, A and B) is associated with the following changes in other climate parameters: (i) cloud amount (Fig. 4A) shifts from values of  $\sim 65$  to  $\sim 45\%$  (mean change,  $-1.7\%$ ); (ii) UTH (Fig. 4B) shifts from values of  $\sim 35$  to  $\sim 15\%$  (mean change,  $-1.5\%$ ); (iii) SW flux (6) shifts from values of  $\sim 75 \text{ W m}^{-2}$  to  $\sim 60 \text{ W m}^{-2}$  (mean change,  $-1.2 \text{ W m}^{-2}$ ); (iv) vertical velocity (6) values become slightly more positive [that is, stronger downward (mean change,  $7.6 \times 10^{-4} \text{ Pa s}^{-1}$ )]; and (v) SAT (6) increases slightly (mean change,  $0.083^\circ\text{C}$ ). Thus, stronger subtropical subsidence dries the upper troposphere and clears clouds, causing the emitted thermal flux to increase and the reflected sunlight to decrease.

The equatorial zone contains areas of both strong upwelling (the rising branch of the Hadley-Walker cell) and strong downwelling (the sinking branch of the Walker cell), and thus changes in Walker cell strength are manifested as changes in the occurrence of extreme high and low values of the various parameters relative to midrange values. For example, LW flux occurrences of midrange values ( $\sim 260 \text{ W m}^{-2}$ ) shift to both lower ( $\sim 230 \text{ W m}^{-2}$ ) and higher ( $\sim 290 \text{ W m}^{-2}$ ) values over time (mean change,  $0.6 \text{ W m}^{-2}$ ) (Fig. 4, C and D). This behavior is accompanied by the following changes in other climate parameters: (i) cloud amount (Fig. 4C) shifts from values of  $\sim 50$  to  $\sim 80\%$  and  $\sim 35\%$  (mean change,  $-0.33\%$ ); (ii) UTH

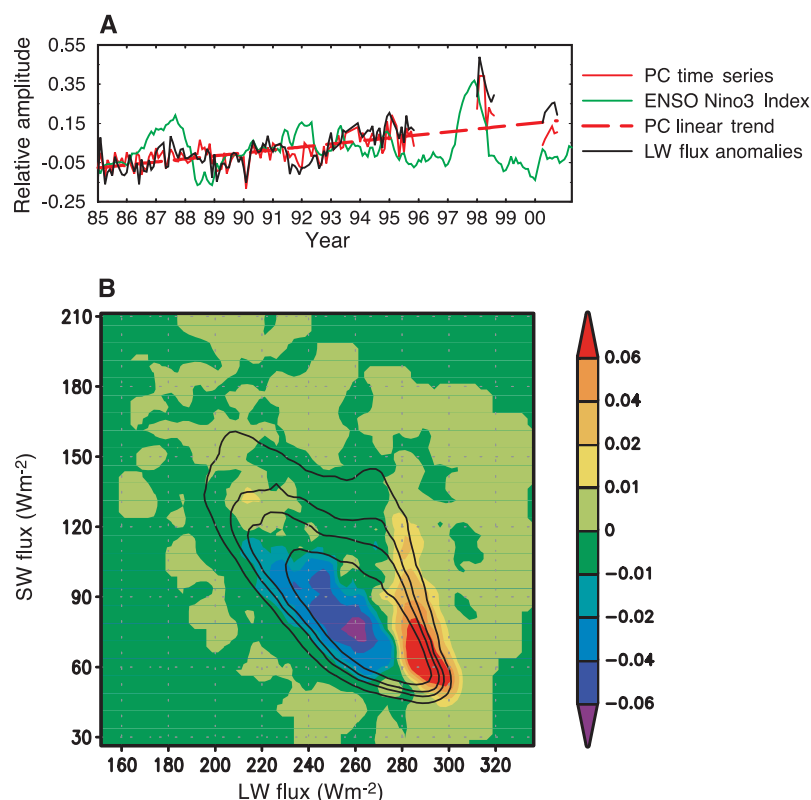


**Fig. 2.** The first mode of the EOF analysis of the SW-LW JFD anomalies. This mode accounts for 15.5% of the total variance. (A) The PC time series (solid red line); the PC linear fit (dashed red line, slope  $3.7 \text{ W m}^{-2}$  per decade); the 30°S–30°N mean LW flux anomalies time series (black line); and the NINO3 ENSO index (green line). The linear correlation coefficient (CC) between the PC and LW flux anomalies is 0.88, and the CC between the LW flux anomalies and the ENSO index is  $-0.10$ . (B) The JFD pattern. The color bar shows the relative change in the JFD domain along the PC time series, whereas the contour is the long-term mean JFD pattern. Negative values indicate pairs of (SW and LW) flux values whose frequency of occurrence has decreased over the analyzed time interval, and positive values indicate pairs of flux values whose frequency of occurrence has increased over the analyzed time interval.

## REPORTS

(Fig. 4D) shifts from values of  $\sim 35$  to  $\sim 50\%$  and  $\sim 20\%$  (mean change,  $-0.20\%$ ); (iii) SW flux ( $\delta$ ) shifts from values of  $\sim 75 \text{ W m}^{-2}$  to  $\sim 60 \text{ W m}^{-2}$ , with no systematic changes at the higher values that correspond to already optically thick clouds (mean change,  $-0.55 \text{ W m}^{-2}$ ); (iv) strong negative (that is, up-

ward) values of vertical velocity ( $\delta$ ) occur more frequently (mean change,  $-4.0 \times 10^{-4} \text{ Pa s}^{-1}$ ); and (v) SAT ( $\delta$ ) warms (mean change,  $0.083^\circ\text{C}$ ).

The equatorial region behavior implies that the rising branch of the Hadley-Walker cell and the sinking branch of the Walker cell

have both strengthened over the decade, and this has caused cloudiness and UTH to increase in the rising regions and decrease in the sinking regions. The increased upward motion near the equator combined with increased downwelling in the subtropics indicates a stronger Hadley cell in more recent years. Wielicki *et al.* infer a cloud change from all-sky fluxes, but the clear-sky flux change is too small for them to infer a water vapor change. We detect both UTH and cloud changes because our analysis extends deeper into the subtropics, where the UTH decrease is largest (Fig. 4B), and because changes in the JFD do not always alter the mean value. Near the equator, more frequent large and small UTH values (Fig. 4D) cancel so that the mean UTH barely changes. Cloud amount exhibits qualitatively similar behavior (Fig. 4, A and C), but there is apparently less cancellation of cloud-induced flux changes than of clear-sky flux changes near the equator. The changes we observe are consistent with previous research on the variability of cloud cover (13), water vapor (14), and SAT (15), but until now it has not been possible to separate the longer term Hadley-Walker circulation variability from ENSO.

Ocean temperature observations (19) show a strong warming of the world ocean during the mid-1990s, caused by a combination of multidecadal warming of the Atlantic and Indian Oceans and a positive extreme in a possible interdecadal oscillation of Pacific Ocean heat content (20–22). Observed tropical lower tropospheric lapse rate changes since 1980 (23) are consistent with our results. Increased adiabatic warming due to stronger Hadley-Walker cell subsidence should steepen the lower tropospheric lapse rate in most locations. The possibility that lapse rates were decreasing instead before 1980 (23) suggests that the observed intensification of the Hadley-Walker cell may be due to natural variability on decadal or longer time scales rather than to a forced climate change; however, the length of the satellite data record is too short to distinguish between these two driving mechanisms.

### References and Notes

1. B. A. Wielicki, R. D. Cess, M. D. King, D. A. Randall, E. F. Harrison, *Bull. Am. Meteorol. Soc.* **77**, 853 (1996).
2. B. R. Barkstrom, G. L. Smith, *Rev. Geophys.* **24**, 379 (1986).
3. B. A. Wielicki *et al.*, *Science* **295**, 841 (2002). Wielicki *et al.* analyze the  $20^\circ\text{S}$ – $20^\circ\text{N}$  latitude range, whereas we consider the  $30^\circ\text{S}$ – $30^\circ\text{N}$  region. Thus, the details of our time series trends and theirs are slightly different.
4. For additional information on the CERES TRMM data, see CERES ES4 TRMM Data Quality Summary ([http://eosweb.larc.nasa.gov/PRODOCS/ceres/ES4/Quality\\_Summaries/CER\\_ES4\\_TRMM-PFM\\_Edition1.html](http://eosweb.larc.nasa.gov/PRODOCS/ceres/ES4/Quality_Summaries/CER_ES4_TRMM-PFM_Edition1.html)).
5. For additional information on the CERES Terra data, see CERES ES4 Terra Data Quality Summary ([http://eosweb.larc.nasa.gov/PRODOCS/ceres/ES4/Quality\\_Summaries/CER\\_ES4\\_Terra\\_Edition1.html](http://eosweb.larc.nasa.gov/PRODOCS/ceres/ES4/Quality_Summaries/CER_ES4_Terra_Edition1.html)).
6. Supplementary Web material is available on *Science*

**Fig. 3.** The PC time series associated with the combined JFD EOF. (A) The first mode PC time series (red line) of the subtropical region data and the  $30^\circ\text{S}$ – $30^\circ\text{N}$  mean LW flux anomalies (green line). This mode accounts for 9.3% of the total variance. The CC between the PC and the LW anomalies is 0.79, and the PC trend is confident at the 99% level (24). (B) The second mode PC time series (red line) of the equatorial region data and the  $30^\circ\text{S}$ – $30^\circ\text{N}$  mean LW flux anomalies (green line). This mode accounts for 5.5% of the total variance. The CC between the PC and the LW anomalies is 0.64, and the PC trend is confident at the 89% level. The first equatorial mode PC (not shown) shows no decadal trend and is modestly correlated with NINO3.

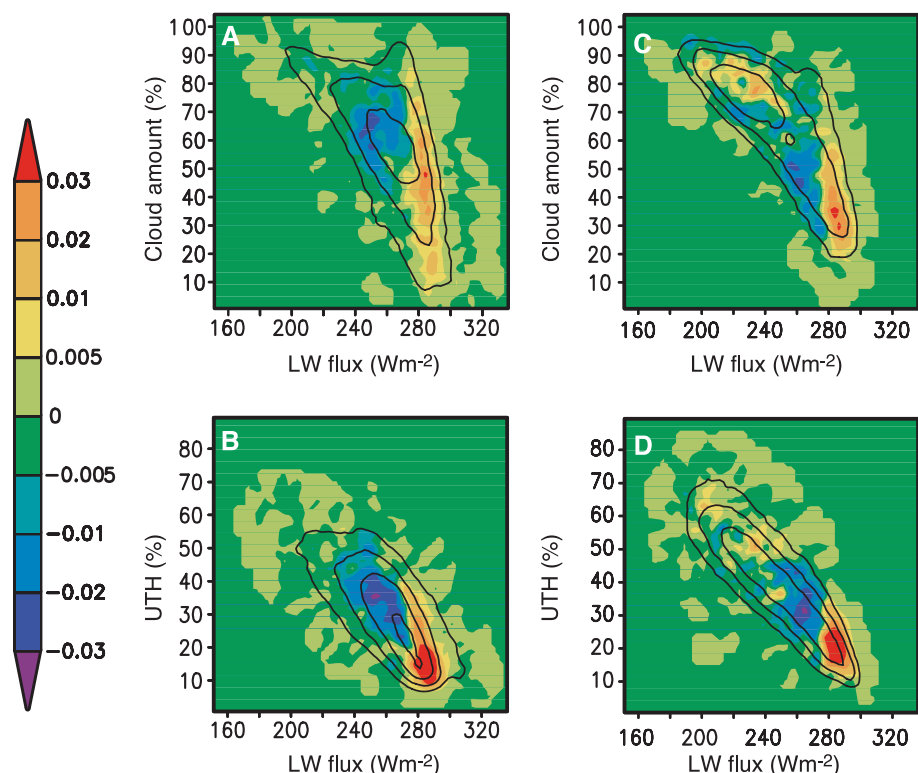
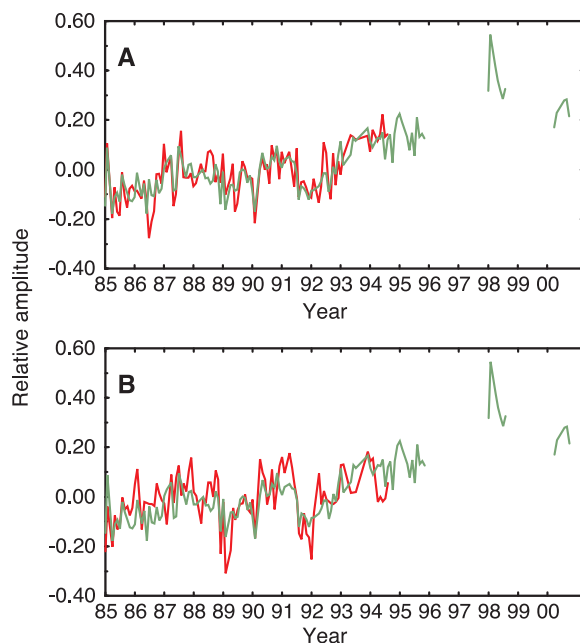


**Fig. 4.** JFD patterns of the combined JFD EOF analyses. (A) Cloud amount–LW flux of the first mode of the subtropical region data. (B) UTH–LW flux of the first mode of the subtropical region data. (C) Cloud amount–LW flux of the second mode of the equatorial region data. (D) UTH–LW flux of the second mode of the equatorial region data.

# Evidence for Large Decadal Variability in the Tropical Mean Radiative Energy Budget

Bruce A. Wielicki,<sup>1\*</sup> Takmeng Wong,<sup>1</sup> Richard P. Allan,<sup>2</sup>  
 Anthony Slingo,<sup>2</sup> Jeffrey T. Kiehl,<sup>3</sup> Brian J. Soden,<sup>4</sup>  
 C. T. Gordon,<sup>4</sup> Alvin J. Miller,<sup>5</sup> Shi-Keng Yang,<sup>5</sup>  
 David A. Randall,<sup>6</sup> Franklin Robertson,<sup>7</sup> Joel Susskind,<sup>8</sup>  
 Herbert Jacobowitz<sup>9</sup>

It is widely assumed that variations in Earth's radiative energy budget at large time and space scales are small. We present new evidence from a compilation of over two decades of accurate satellite data that the top-of-atmosphere (TOA) tropical radiative energy budget is much more dynamic and variable than previously thought. Results indicate that the radiation budget changes are caused by changes in tropical mean cloudiness. The results of several current climate model simulations fail to predict this large observed variation in tropical energy budget. The missing variability in the models highlights the critical need to improve cloud modeling in the tropics so that prediction of tropical climate on interannual and decadal time scales can be improved.

Earth's climate system is driven by a radiative energy balance between the solar or shortwave (SW) radiation absorbed by Earth and the thermal infrared or longwave (LW) radiation emitted back to space. The balance both modifies and is modified by the components of the Earth-atmosphere system such as clouds, the surface, and the atmosphere (*1*). Therefore, the TOA radiation budget is crucial in determining climate variability and feedbacks, whereas its measurement provides a severe test of our ability to represent physical processes important for simulations of future climate.

A new set of Earth radiation balance data is now being provided by the NASA CERES (Clouds and the Earth's Radiant Energy System) instrument on the Tropical Rainfall Measuring Mission (TRMM) for 8 months in 1998 and by the Terra satellite mission that began in March 2000 and is expected to continue through 2007 (*2, 3*). In addition, with the 16-year record of the Earth Radiation Budget Satellite (ERBS), it is now possible to examine 22 years of accurate satellite observed broadband radiative fluxes (*4–6*).

Anomalies in tropical mean broadband thermal LW flux emitted by the Earth have been determined from this 22-year record and are shown in Fig. 1.

Calibration absolute accuracies for the seven broadband radiometers in Fig. 1 are estimated to be roughly 1% for the pre-CERES instruments and 0.5% for the newer records. The anomaly results during data overlap periods from all instruments are consistent to within about  $1 \text{ Wm}^{-2}$  or about 0.5% of the  $253 \text{ Wm}^{-2}$  ERBE tropical mean LW flux. Only stability of calibration enters the anomaly record for the ERBS nonscanner (NS) data, whereas both stability and absolute calibration affect the scanner (SC) anomaly records from five different instruments.

The LW anomaly record in Fig. 1 shows much larger variations than expected, especially for the 1997/1998 El Niño event, which reaches a tropical mean anomaly of  $8 \text{ Wm}^{-2}$ , the largest seen to date. Other notable short-term anomalies are the rapid drop in LW flux resulting from the Mount Pinatubo Eruption in 1991 (*7*), followed by the expected 2-year recovery period as the volcanic aerosols are removed from the stratosphere and upper troposphere. Although the 1983 El Niño event is thought to be comparable in magnitude to the 1997/1998 El Niño, there is no comparable tropical mean LW flux anomaly. A plausible hypothesis is that the earlier 1982 El Chichon eruption caused a reduction in LW flux similar to that from the Mount Pinatubo Eruption in 1991. The resulting LW fluxes in 1982 to 1984 would, in this case, be a partial cancellation of the El Chichon and El Niño signals. But the most surprising result in the figure is an apparent drop of about  $2 \text{ Wm}^{-2}$  in LW

Online at [www.sciencemag.org/cgi/content/full/295/5556/838/DC1](http://www.sciencemag.org/cgi/content/full/295/5556/838/DC1).

7. J. P. Peixoto, A. H. Oort, *Physics of Climate* (American Institute of Physics, New York, 1992).
8. Anomalies are defined as the deviation from the mean annual cycle for the years 1985–1993.
9. The commonly used NINO3 ENSO index is defined as the  $150^{\circ}\text{W}$ – $90^{\circ}\text{W}$   $5^{\circ}\text{S}$ – $5^{\circ}\text{N}$  average sea surface temperature anomaly.
10. M. Chelliah, P. Arkin, *J. Clim.* **5**, 371 (1992).
11. The two-dimensional JFD is a matrix whose elements contain the frequency of occurrence of various pairs of parameter values (in this case, SW and LW fluxes). In this research, all data sets are monthly means and are mapped to  $5^{\circ} \times 5^{\circ}$  spatial resolution. The JFDs are calculated on the basis of these data sets.
12. The mean annual cycle is calculated from the composite 1985–1993 JFD, and then the JFD anomalies time series is derived. The JFD anomalies matrix is smoothed before EOF decomposition. Through EOF decomposition, we obtain a series of modes arranged in decreasing order of the fractions of variance that they can explain. Each mode has two components: The EOF, the eigenvector of the covariance matrix, represents the JFD pattern of the mode; the PC, the time series of the projection of each month's JFD anomaly on this EOF, represents the temporal variation.
13. W. B. Rossow, R. A. Schiffer, *Bull. Am. Meteorol. Soc.* **80**, 2261 (1999).
14. J. J. Bates, D. L. Jackson, *Geophys. Res. Lett.* **28**, 1695 (2001).
15. J. Hansen, R. Ruedy, J. Glasco, M. Sato, *J. Geophys. Res.* **104**, 30997 (1999).
16. Omega is the standard meteorological symbol for the vertical velocity in pressure coordinates in units of  $\text{Pa s}^{-1}$ . Its direction is upward when its value is negative.
17. E. Kalnay et al., *Bull. Am. Meteorol. Soc.* **77**, 437 (1996).
18. The JFD anomalies of the five parameters and LW flux are combined to construct new two-dimensional matrices. After the EOF analysis is applied to the time series of the new matrices, the resulting EOF of each mode is separated back into five individual JFD patterns, one for each parameter and the LW flux. The five JFD patterns share the PC time series together; that is, a given mode depicts related variations in all the parameters and fluxes. As a separate test, we also performed an EOF analysis for each parameter and for LW flux JFD anomalies individually for the entire tropics. The correlations of the resulting PCs with the tropical mean LW anomalies time series are as follows: cloud amount–LW, 0.75; UTH–LW, 0.75; omega–LW, 0.86; and SAT–LW, 0.93.
19. S. Levitus, J. I. Antonov, T. P. Boyer, C. Stephens, *Science* **287**, 2225 (2000).
20. M. Latif, R. Kleeman, C. Eckert, *J. Clim.* **10**, 2222 (1997).
21. D. E. Parker, *Science* **287**, 1216 (2000).
22. S. Power, T. Casey, C. Folland, A. Colman, V. Mehta, *Clim. Dyn.* **15**, 319 (1999).
23. D. J. Gaffen et al., *Science* **287**, 1242 (2000).
24. E. C. Weatherhead et al., *J. Geophys. Res.* **103**, 17149 (1998).
25. Supported by the NASA Tropical Rainfall Measuring Mission and the Department of Energy Atmospheric Radiation Measurement Program. We thank R.-X. Ying, D. Chen, J.-P. Liu, R. A. Ruedy, Y.-C. Zhang, and L. DelValle for their help at various stages of this work; B. A. Wielicki and K.-M. Xu for their comments on the manuscript; and B. A. Wielicki for suggesting the test to confirm that calibration shifts cannot explain the results. The ERBE, CERES, and the International Satellite Cloud Climatology Project data were obtained from the NASA Langley Research Center Atmospheric Sciences Data Center. J. J. Bates and D. L. Jackson provided the HIRS UTH data. The NCEP Reanalysis data are provided by the National Oceanic and Atmospheric Administration–Cooperative Institute for Research in Environmental Sciences Climate Diagnostics Center, Boulder, CO, USA, from their Web site at <http://www.cdc.noaa.gov/>.

<sup>1</sup>NASA Langley Research Center, Hampton, VA 23681, USA. <sup>2</sup>Hadley Centre, Met Office, Bracknell, RG12 2SY, UK. <sup>3</sup>National Center for Atmospheric Research, Post Office Box 3000, Boulder, CO 80303, USA. <sup>4</sup>GFDL/NOAA, Princeton University, Post Office Box 308, Princeton, NJ 08542, USA. <sup>5</sup>NOAA Climate Prediction Center/NCEP, Camp Springs, MD 20746, USA. <sup>6</sup>Colorado State University, Fort Collins, CO 80523, USA. <sup>7</sup>NASA Marshall Space Flight Center, Huntsville, AL 35812, USA. <sup>8</sup>NASA Goddard Space Flight Center, Greenbelt, MD 20771, USA. <sup>9</sup>NOAA/NESDIS, Camp Springs, MD 20746, USA.

\*To whom correspondence should be addressed. E-mail: [b.a.wielicki@larc.nasa.gov](mailto:b.a.wielicki@larc.nasa.gov)